Int. J. Electrochem. Sci., 16 **(2021)** 151028, doi: 10.20964/2021.01.50

International Journal of
ELECTROCHEMICAL
SCIENCE
www.electrochemsci.org

Synthesis and Wear Characterization of Ultrasonic Electrodeposited Ni-TiN Thin Coatings

Tianxiang Liu[1], Chaoyu Li[2], Qiang Li[2], Liangzhao Li[3], Fafeng Xia[2], Haiyan Xing[2], Chunyang Ma[2]*

[1] College of Engineering, Heilongjiang Bayi Agricultural University, Daqing 163319, China;
[2] College of Mechanical Science and Engineering, Northeast Petroleum University, Daqing 163318, China;
[3] School of Chemistry & Environmental Engineering, Hanshan Normal University, Chaozhou 521041, China
[*]E-mail: chunyangandma1@163.com

Received: 1 October 2020 / *Accepted:* 12 November 2020 / *Published:* 30 November 2020

This work describes the use of a modified Watt nickel bath to prepare pure Ni and Ni–TiN thin coatings by the application of ultrasonic electrodeposition (UE) under pulse current (PC) conditions. X-ray diffraction (XRD), transmission electron microscopy (TEM), scanning electron microscopy (SEM), scanning probe microscopy (SPM) were used to investigate the influences of ultrasonic intensity on phase composition, surface topography, and microscopic structure. The Vickers hardness, wear resistance of Ni and Ni–TiN coatings, and coefficient of friction were also tested. The TEM, SEM, and SPM results showed that under the ultrasonic wave with the intensity of 30 W/cm^2, Ni-TiN coatings exhibited a glossy and uniform surface topography. For NT-2 coating with a superficial area of 4.102 μm^2, the root means square (*Rms*) roughness was 36.825 nm and the arithmetic mean roughness (*Ra*) was 22.658 nm. The average size of Ni grains was 47.1 nm, whereas that of TiN nanoparticles was observed as 23.2 nm. The diffraction angle of the coatings with disparate coating parameters in the XRD analysis was found to be similar to the Ni phase, however, the intensity of diffraction varied. The microhardness experiment showed that the minimum microhardness of the Ni film was 387.6 HV. Furthermore, the maximum microhardness value got from the Ni-TiN coating under the ultrasonic wave with an intensity of 30 W/cm^2 was 912.1 HV. Wear and friction evaluation showed that the loss in weight of Ni-TiN coatings performed with 30w/cm^2 ultrasonic intensity was the smallest, and the average friction coefficient was measured to be 0.39, thus exhibiting good resistance to wear.

Keywords: Preparation; 3D surface morphology, Ni-TiN thin coating; Microstructure, Wear assessment

1. INTRODUCTION

TiN ceramic material has been widely known for its use in machinery, electronics, and chemical industry for its excellent chemical and physical properties [1-3]. Generally, to enhance the performance,

particularly in terms of microhardness, antioxidant capacity, anti-corrosion property and wear resistance, TiN micro-/nano-particles are inset in metal coatings. As a result, metal-based TiN thin coatings have emerged as an area of extensive investigation during the past few years [4-6]. In several studies, the nickel-based coatings, including Ni-SiC, Ni-TiN, and Ni-Al_2O_3, have been used as a result of their prominent performance [7-9]. Ultrasonic electrodeposition (UE) is an advantageous special working technology for the fabrication of ceramic, metal, or organic thin coatings in alloy and metal substrates. In this study, ultrasonic dispersion is put to use for reducing the agglomeration of micro- and nano-particles, to improve the suspension of particles in the electroplating bath, to cut down the porosity of the coatings affected by the evolution of hydrogen. In view of some contemporary reports, the arrangement of nickel-based thin coatings gained based on the UE approach can improve the properties of the coatings, and refine the microstructure of the coating. Xia *et al.* [10] confirmed that soft ultrasonic treatment of Ni-TiN coatings resulted in the uniform interspersion of TiN particles. Ni-SiC coatings from an electrolytic solution of nickel sulfamate including SiC particles have been reported by Gyawali *et al.* [11]. Ni–SiC coatings were integrated by Li *et al.* [12] using the technique of ultrasonic electrodeposition. Although much work has been done on the deposition of pulse-current (PC), direct-current (DC), or UE, relatively little research has been done regarding the provision and wear evaluation of supersonic electro-plating Ni–TiN thin coatings. In the current study, thin coatings based on pure Ni and Ni–TiN were prepared by the UE method using a modified Watt nickel bath under PC condition (UEPC). The phase composition, the microstructure as well the impact of ultrasonic wave intensity on the surface topography were assessed using X-ray diffraction, transmission electron microscopy, scanning electron microscopy, and scanning probe microscopy. Besides, we carried out a detailed evaluation of the friction properties, wear-resistance, and the distinctions in Vickers hardness number of Ni and Ni–TiN thin coatings.

2. EXPERIMENTAL

2.1 Sample preparation

A corrective Watt nickel bath was used to prepare pure Ni and Ni-TiN thin coatings (with a thickness of ~60 μm). TiN nanoparticles having a 20 nm mean size were used to form the Ni-TiN thin coatings. A scheme illustrating the standard electrodeposition device is shown in Fig. 1. It comprises an ultrasonic generator (XL-500), a numerically controlled pulse power unit (SMD-300), an A3 steel substrate, a 99.99% pure nickel plate, and a plating tank. The nickel plate was separated from the A3 steel substrate by a distance of 15 mm during UEPC. The pulse current was created between the nickel plate and A3 steel substrate using the numerically controlled pulse power source. The ultrasonic wave with a frequency of 40 kHz and intensity values varying between 0 W/cm^2 to 30 W/cm^2 were generated. Table 1 elaborates on the coating conditions and chemical constituents of unmixed Ni and Ni-TiN thin coatings. The solution for plating was subjected to ultrasounds (ultrasonic power 250 W) 10 min before utilizing for distributing TiN nanoparticles uniformly within the suspension in the plating bath.

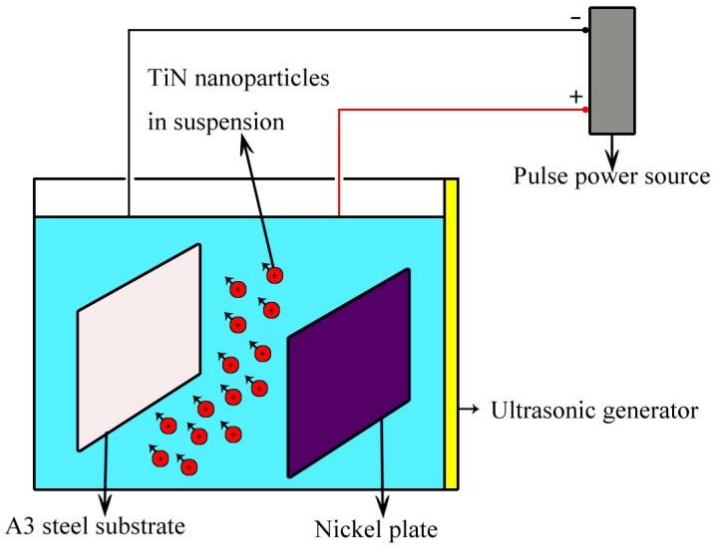

Figure 1. Schematic diagram of the standard electrodeposition device.

Table 1. Electrolyte composition and plating conditions for prefabricating Ni-TiN thin coatings.

Sample	Ni coating	Ni-TiN thin coating (NT-1)	Ni-TiN thin coating (NT-2)
$NiSO_4 \cdot 6H_2O$ (g/l)	290	290	290
$NiCl_2 \cdot H_2O$ (g/l)	32	32	32
H_3BO_3 (g/l)	28	28	28
TiN nanoparticles (g/l)	8	8	8
Surfactant (sodium dodecyl benzene) (mg/l)	50	50	50
Plating temperature (°C)	45	45	45
Current density (A/dm^2)	6	6	6
pH	4.5	4.5	4.5
Ultrasonic intensity (W/cm^2)	30	0	30
Electroplating time (min)	60	60	60

2.2 Analysis and characterization

Deionized water was used to wash the specimens following UPEC which were then subjected to ultrasonication for 6 min to get rid of the superficial TiN nanoparticles. A GZ-60 type oven was used to dry samples. The microstructures and overall shape of the Ni–TiN thin coatings were examined using transmission electron microscopy (TEM, Tecnai-G2-20-S-Twin), scanning electron microscopy (SEM, JSM-6460LV), and scanning probe microscopy (SPM, Nanoscope IIIa). A Rigaku D/Max-2400 type X-ray diffraction instrument (XRD, Cu Ka wavelength of 1.5418 Angstroms, 2°/min scan rate) was employed to determine the phase compositions of the coatings. The following equation was used to determine the average sizes of the Ni–TiN coatings:

$$D = \frac{0.94\lambda}{B\cos\theta} \qquad (1)$$

Where the mean diameter of the grain is referred to as D, θ refers to the Bragg angle, λ stands for Cu Ka wavelength, and B is the full width at half maximum of the peak at an angle θ.

A THV-1000 microhardness tester was used to investigate the Vickers microhardness. The loading time and loading capacity were respectively found to be 10 s and 100 gf. A MR-H6A type non-lubricated wear testing machine was utilized to estimate the wear resistance of the thin coatings based on Ni and Ni–TiN coatings as well as friction coefficient. The abrasion tests were carried out on a quenched steel ball with a diameter of 4 mm, 200 r/min sliding velocity, and a 100 gf external load sustaining 180 min. Before and after each test, the Ni–TiN coating was washed by ultrasonic within deionized water. An electrical balance of LD510-2 type having an accuracy of 0.01 mg was used to compute the loss of film weight. Meanwhile, the 3D-2A type optical surface profile equipment was used to observe the 3D surface structure of the Ni–TiN thin coatings.

3. RESULTS AND DISCUSSION

3.1 Surface morphology and microstructure

3.1.1 SEM analysis

The SEM pictures of the Ni and Ni-TiN thin coatings prepared by UEPC deposition under different parameters for plating are presented in Fig. 2.

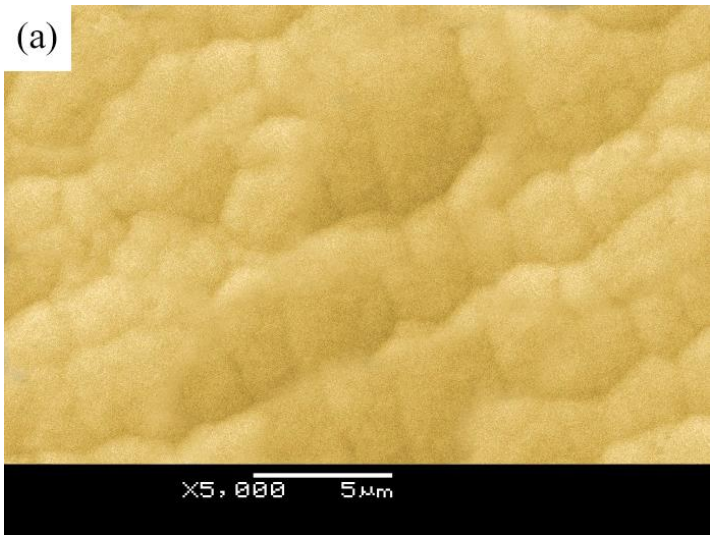

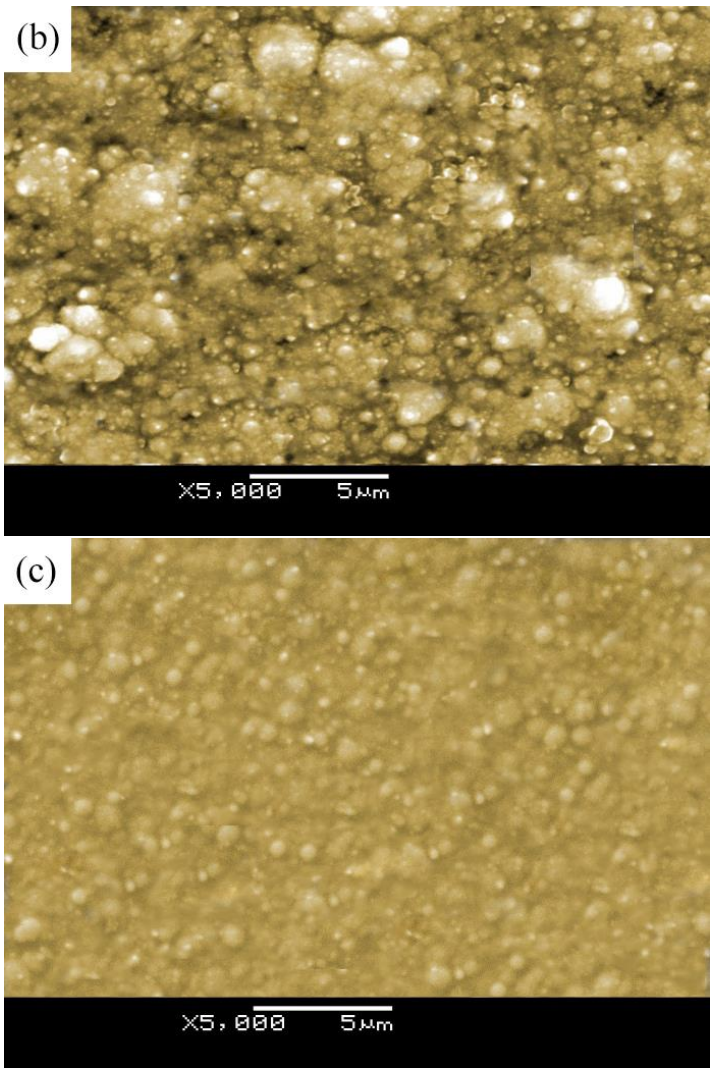

Figure 2. SEM pictures of UEPC-deposited Ni and Ni-TiN thin coatings: (a) Ni coating, (b) NT-1 coating, (c) NT-2 coating.

Ni coatings were noticed to have attained a large crystalline structure resembling that of cauliflower in the microscopic state under 30 W/cm^2 ultrasonic intensity (Fig. 2a). In contrast, the medium-sized crown shape appeared on the NT-1 thin coating (Fig. 2b). On the contrary, at 30 W/cm^2 ultrasonic intensity, Ni-TiN thin coatings had a good, glossy, and uniform surface topography. TiN nanoparticles in large numbers were uniformly diffused in the Ni-TiN thin coating (Fig. 2c).

3.1.2 SPM survey

The influence of intensity of ultrasonic waves upon the SPM pictures of the thin coatings based on Ni and Ni-TiN thin coatings prepared by the method is illustrated in Fig. 3. Different surface structure and surface roughness numbers of the thin coatings based on Ni and Ni-TiN manifested. The Ni coating shown in Fig. 3a revealed a rough and smooth surface structure, while the arithmetic mean roughness (*Ra*) and root-mean-square roughness (*Rms*) were 39.471 nm and 48.325 nm, respectively. On the contrary, compared with Ni coating, NT-1 coating has a higher roughness surface and lower micrograin

size. The *Ra* and *Rms* measures of the film were 52.972 nm and 65.965 nm, respectively (Fig. 3b). However, the Ni-TiN coating acquired at 30 W/cm^2 ultrasonic intensity had a glossy and uniform surface topography. The values of *Ra* and *Rms* for the film having a surface area of 4.102 μm^2 were 22.658 nm and 36.825 nm, respectively (Fig. 3c).

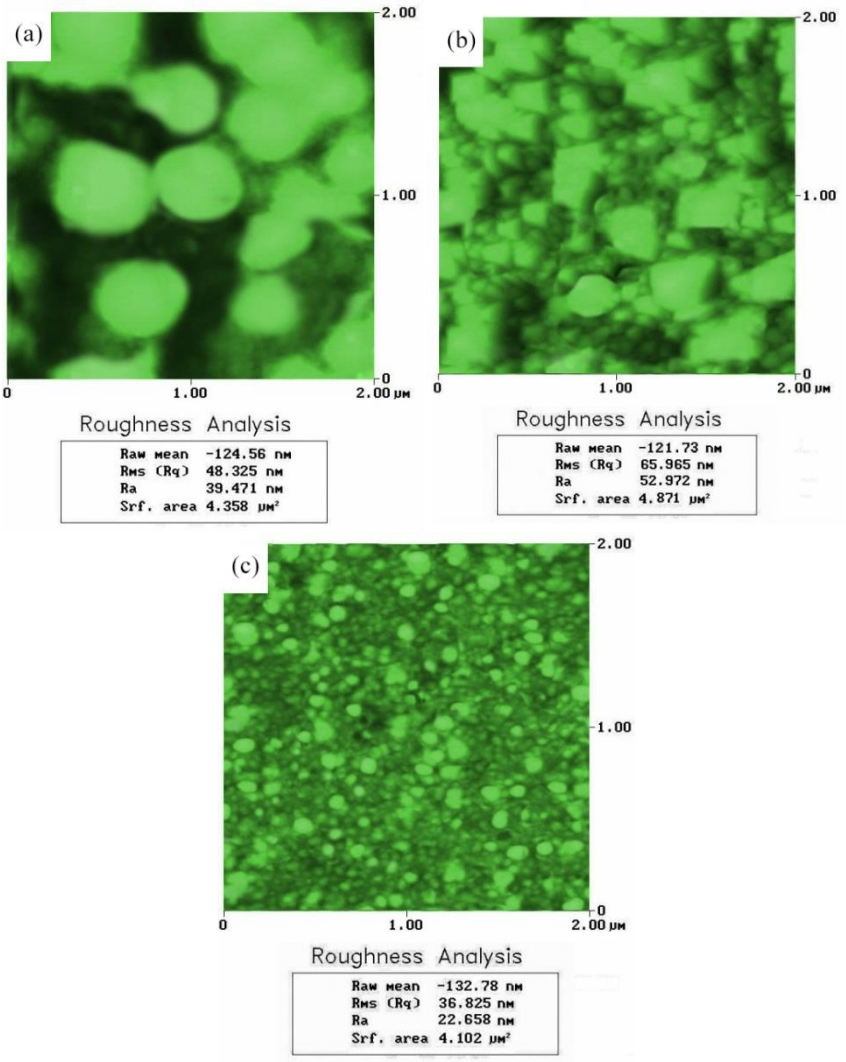

Figure 3. SPM pictures of UEPC-deposited Ni and Ni-TiN thin coatings: (a) Ni coating, (b) NT-1 coating, (c) NT-2 coating.

3.1.3 TEM measurement

The TEM graphics of Ni and Ni-TiN thin coatings deposited by UEPC through different parameters for plating are shown in Fig. 4a~c. Fig. 4a'~c' respectively shows the nickel grains in terms of their statistical distribution in the coatings under investigation, attained by UEPC deposition. Compared with NT-1 and NT-2 coatings, the size of Ni grains in the coatings with 30 W/cm^2 ultrasonic intensity was bigger while the Ni grains were ~285.2 nm in diameter on average. On the contrary, the

NT-2 thin coating showed a homogeneous and favorable microstructure; however, the Ni particles and TiN nanoparticles had an average diameter of about 47.1 nm and 23.2 nm.

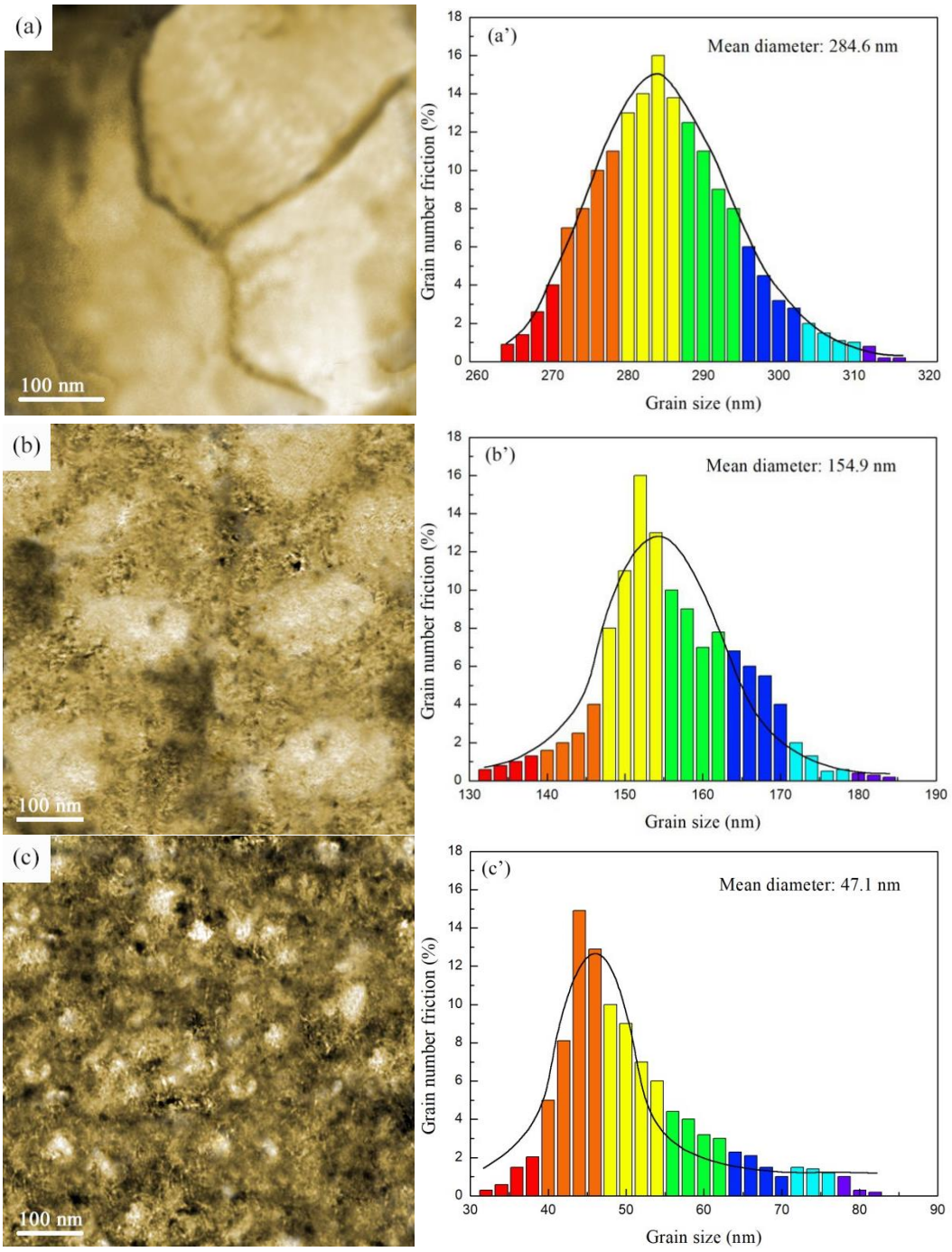

Figure 4. TEM graphics of UEPC-deposited Ni and Ni-TiN thin coatings: (a) Ni coating, (b) NT-1 coating, (c) NT-2 coating.

3.1.4 Coating formation mechanism

Gugliemi's absorption model verifies the above phenomena as shown in Fig. 5 [13]. In the process of preparing the nickel coating, the Ni grains in the Ni coating grew big very fast with the action of ultrasound under conditions where TiN nanoparticles were not cited, leading to the appearance of a large-sized crown crystal structure, similarly to the shape of cauliflower. Adversely, in the process of preparing Ni-TiN coating, when medium-intensity ultrasonic waves and TiN nanoparticles were applied, the flow of sound produced by the ultrasonic generator caused the TiN nanoparticles to form a uniformly distributed suspension in the bath [14]. As a consequence, the results respectively show that under the influence of the electric field and ultrasonic force generated by impulse power and the supersonic generator, the TiN nanoparticles were weakly deposited on the surface of the substrate. Lastly, Ni atoms trapped the TiN nanoparticles present on the surface of the substrate and thus embedded them in the Ni-TiN coating. It was worth noting that the nucleation number of Ni particles was effectively increased by TiN nanoparticles and the grain development could be restrained (Figs. 2b, 3b, and 4b). Besides, the Ni-TiN thin coating made at an ultrasonic wave of 30 W/cm^2 intensity bears a good, glossy, and uniform surface topography owing to the ultrasonic intensity, which in reality is beneficial to the uniform distribution of TiN nanoparticles in the coating [15]. Additionally, the phenomenon of TiN particles inhibiting the growth of Ni grains in the coating was found to be enhanced [16]. Furthermore, the glossy and uniform surface topography of the Ni-TiN thin coating is illustrated in Figs 2c, 3c, and 4c.

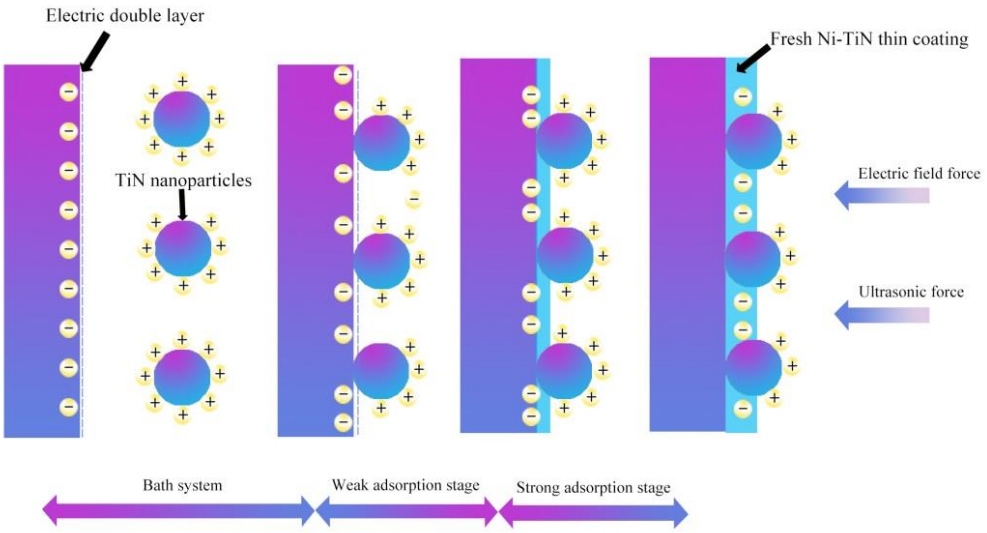

Figure 5. UEPC-deposited diagrams of Ni-TiN thin coatings between Ni irons and TiN nanoparticles.

3.2 Phase structure analysis

Fig. 6a shows the XRD images of the Ni, while the Ni-TiN thin coatings prepared by UEPC deposition under different coating parameters are shown in Figs. 6b and 6c. The X-ray diffractometer scans at angles ranging from 30° to 80°. The results showed that the diffraction angle for coatings made

using various coating parameters was basically identical for the different diffraction intensities. The Ni film showed only the Ni-phase owing to insufficient TiN nanoparticles in the bath (Fig. 6a). Thus, respective values of the diffraction crust of the Ni phase corresponding to (1 1 1), (2 0 0), and (2 2 0) were 44.6°, 52.4°, and 76.8°, Ni and TiN phases primarily gave rise to the Ni-TiN thin coatings (Figs. 6b~c). The Ni phase diffraction peaks kept pace with the Ni coating, while in the case of TiN phase, the diffraction corresponding to (1 1 1), (2 0 0), and (2 2 0) had a value of 36.64°, 42.62°, and 61.80°. In the light of the X-ray diffraction spectrum, Eq. (1) was used to determine the mean grain diameters of the TiN and Ni phases in the NT-2 thin coating and the respective results were ~ 48.8 nm and ~27.1 nm. This outcome was nearly the same as the result obtained by TEM.

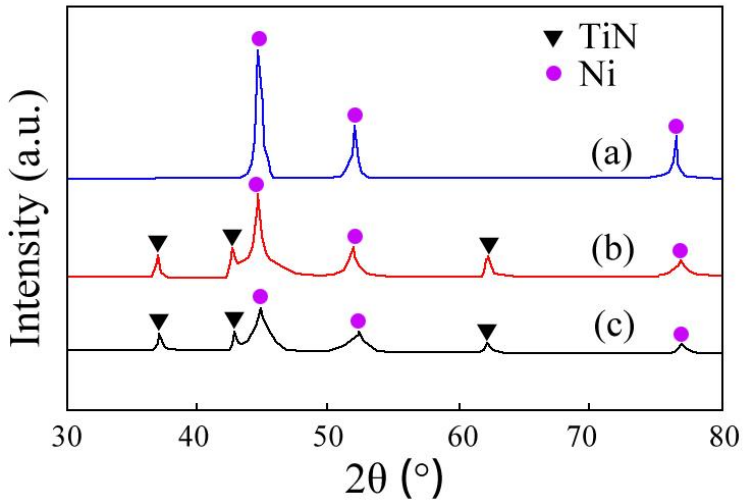

Figure 6. XRD images of UEPC-deposited Ni and Ni-TiN thin coatings: (a) Ni coating, (b) NT-1 coating, (c) NT-2 coating.

3.3 Investigation of Mechanical properties

The data regarding microhardness of the Ni and Ni-TiN thin coatings deposited by UEPC through different coating parameters are shown in Fig. 7. The results showed that the minimum microhardness value of the Ni film was 387.6 HV. Likewise, under ultrasonic wave with 30 W/cm^2 intensity, the Ni-TiN coating with the maximum microhardness measure of 912.1 HV was obtained. Besides, the medium microhardness of NT-1 coating was 788.3 HV. The results showed that under the condition of ultrasonic intensity of 30W/cm^2, owing to the proper ultrasonic intensity and diffusion hardening effect of TiN nanoparticles, the microhardness of Ni-TiN coating has the largest value than that of the Ni film and NT-1 coating. Whereas, the microhardness of TiN nanoparticles was larger in comparison to that of the Ni particles, which has the potential to create a significant improvement in the performance of thin coatings comprising Ni-TiN. However, moderate ultrasonic intensity resulted in TiN nanoparticles being uniformly dispersed in the Ni-TiN thin coating [17].

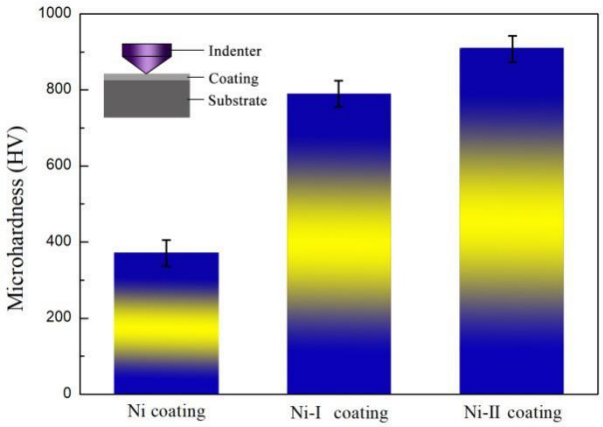

Figure 7. Microhardnesses of UEPC-deposited Ni and Ni-TiN thin coatings: (a) Ni coating, (b) NT-1 coating, (c) NT-2 coating.

3.4 Wear behavior assessment

3.4.1 Detection of Weight loss

The relationship between the weight loss curve and the wear time of the Ni and the Ni–TiN thin coating attained by UEPC deposition was shown in Fig. 8. During the test, the wear loss-gravity curve of the Ni and Ni-TiN thin coatings prepared by UEPC added significantly to the prolonged wear time. Particularly the weight loss of the Ni film increased rapidly with the increase in wear time. Further, under the same value of wear time, the weight loss rate of NT-2 coating was found to be the lowest, whereas that of Ni coating was the highest.

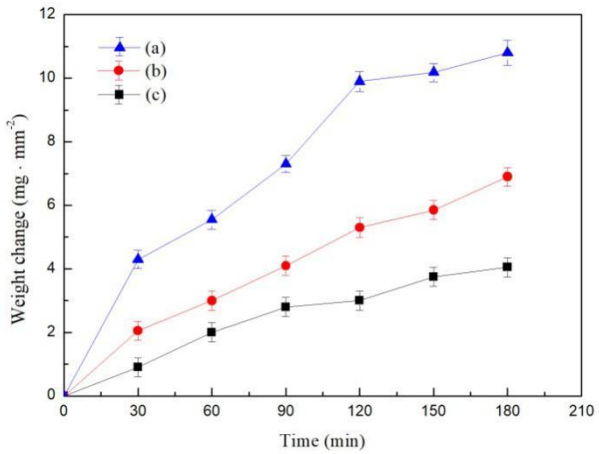

Figure 8. Weight loss curves of UEPC-deposited Ni and Ni-TiN thin coatings: (a) Ni coating, (b) NT-1 coating, (c) NT-2 coating.

As known, the number and allocation of ceramic particles determine the weight losses of Ni-TiN coatings [18]. In comparison with the Ni and NT-1 coatings, the highest TiN content was observed for the NT-2 whereas uniform scattering was observed for the TiN nanoparticles in the NT-2 membrane as evident in Figs. 2~4. The result is the NT-2 coating being improved in terms of wear resistance. The outcome showed that when the ultrasonic intensity was 30 W/cm^2, the rate of weight loss rate for coatings comprising Ni-TIN was the lowest compared to the other two coatings.

3.4.2 Friction coefficient analysis

Fig. 9 shows the friction coefficient curves of nickel and Ni-TiN coatings prepared by UEPC under different coating parameters. The results showed that the coefficient of friction curve slopes of the thin coatings comprising Ni and Ni-TiN quickly added with the increase of sliding distance, and remained stable within a certain range until the end of the wear test. The smallest friction coefficient was observed for the NT-2 coating is the smallest, however, the average friction coefficient was observed to be approximately 0.39. On the contrary, for Ni and NT-1 coatings, the friction coefficients exhibited higher values under the same wear test parameters. This result can be ascribed to the microhardness and surface roughness of the coating [19]. When the microhardness was high and the surface roughness of the coating was low, the friction coefficient was found to be low. Hence, the smallest friction coefficient was observed for the Ni-TiN coating at the ultrasonic intensity of 30 W/cm^2. Through this experiment, it is also obvious that the uniformity in the TiN nanoparticles dispersion in the Ni-TiN coating depends largely on appropriate ultrasonication, thereby forming a good, glossy, and uniform surface topography. The result was a decrease in the friction coefficient of the film.

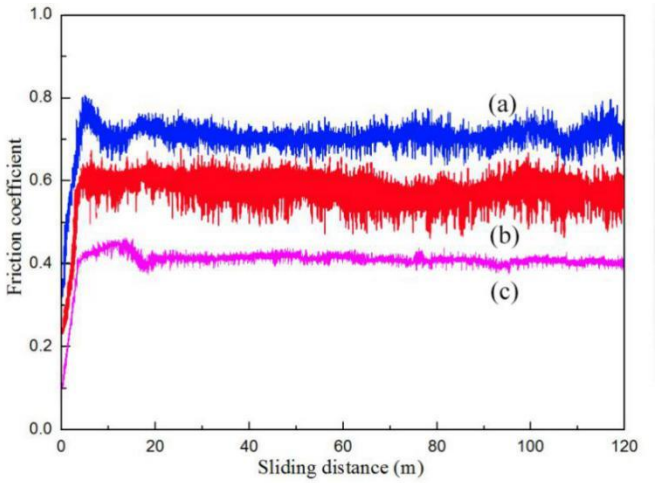

Figure 9. Friction coefficient curves of UEPC-deposited Ni and Ni-TiN thin coatings: (a) Ni coating, (b) NT-1 coating, (c) NT-2 coating.

3.4.3 3D surface morphology observation

The 3D surface morphologies of thin coatings based on Ni and Ni-TiN generated via UEPC after 180 min of abrasion test are presented in Fig. 10. The results show that the worn surface of the thin

coatings manifests there are some clearly visible traces and grooves. In comparison to the Ni-TiN thin coatings, the wear traces of the Ni coating was comparatively deep and wide. Additionally, the NT-2 coating had only slight wear, however, there was serious damage in the NT-1 coating that resulted during wear test from the quenched steel ball. Hence, NT-2 coating had better wear resistance than NT-1 coating. The results also highlighted the importance of a proper ultrasonic intensity to allow TiN particles to be uniformly dispersed in the coatings. The coating structure also became considerably stronger and attained increasing stability, thus exhibiting very high abrasion resistance. Besides, the reasonably distributed TiN in the wear test could expand moderately on the nickel base, which prevented normal loads transferring from the substrate, bringing about a reduction in shear forces between the membrane interface and the steel ball [20]. Therefore, under an ultrasonic intensity of 30 W/cm^2, the Ni-TiN coatings were found to have the best abrasion resistance.

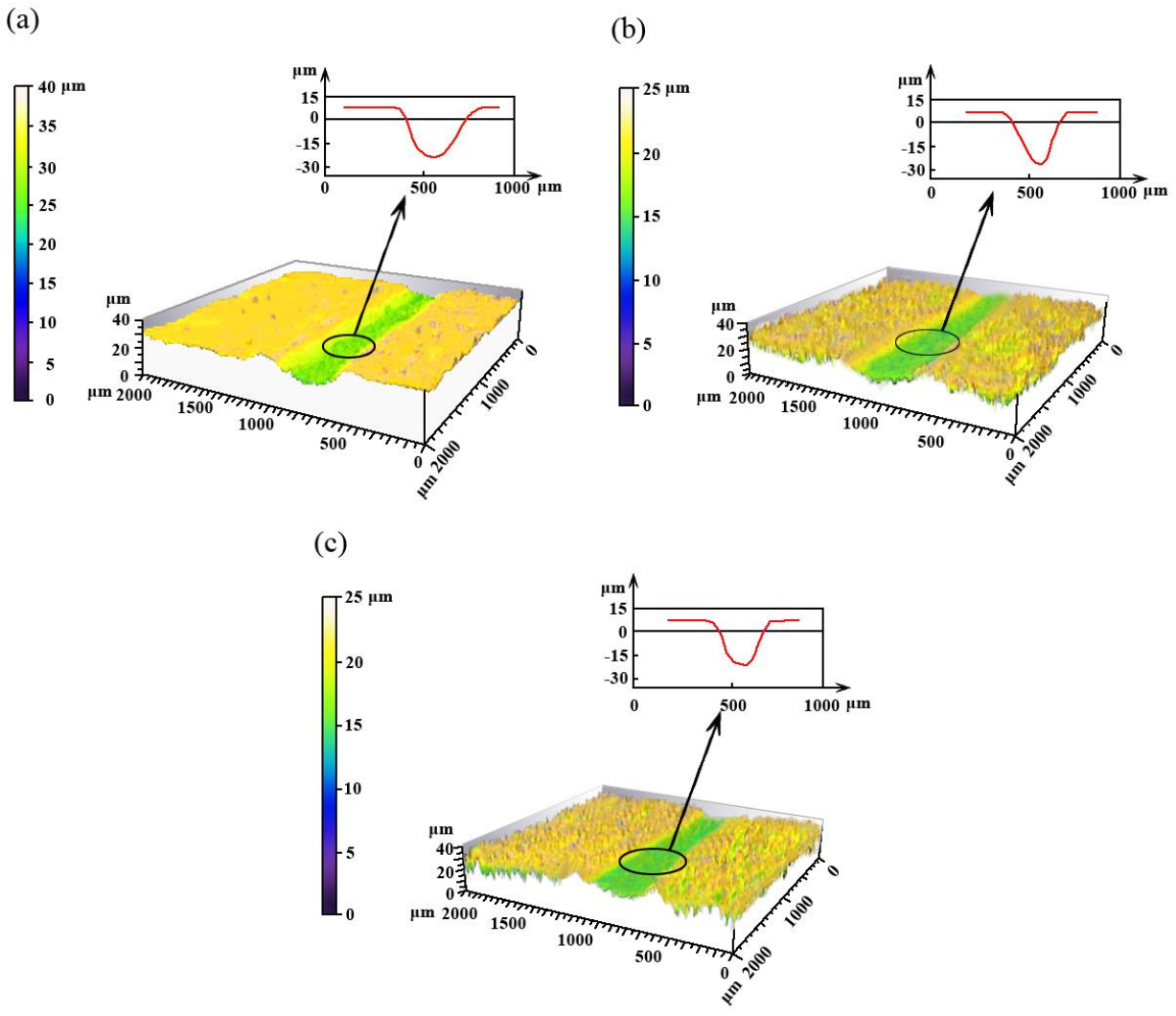

Figure 10. Three-dimensional surface morphologies of the UEPC-produced Ni and Ni-TiN thin coatings subsequently to wear testing for 180 min: (a) Ni coating, (b) NT-1 coating, (c) NT-2 coating.

4. CONCLUSIONS

(1) The surface morphology of the Ni coating is rough and flat, while the value of the arithmetic mean roughness (*Ra*) was estimated to be 39.471 nm and that of root mean square roughness (*Rms*) was found to be 48.325 nm. Contrary to this, The Ni-TiN thin coating prepared under 30 W/cm^2 ultrasonic intensity attained a good, glossy, and uniform surface topography. The *Ra and Rms* of the coating with a surface area of 4.102 μm^2 were 22.658 and 36.825 nm respectively. Besides, the average diameters of Ni grains were observed to be 47.1 nm and that of TiN nanoparticles was 23.2 nm.

(2) The XRD analysis showed that while diffraction intensity was different, the diffraction angle of the coatings made by various coating parameters was the same as that of the Ni phase. Because there were no TiN nanoparticles in the bath, only the Ni phase was manifested in the Ni coating. In contrast, Ni and TiN phases comprised the Ni-TiN thin coatings.

(3) The minimum microhardness value of the Ni coating as obtained in microhardness analysis was found to be 387.6 HV. Furthermore, the Ni-TiN coating with the maximal microhardness measurement of 912.1 HV was obtained under ultrasonic wave under 30 W/cm^2 intensity. In addition, the medium microhardness of Ni-TiN coating obtained by 0 W/cm^2 was 788.3 HV.

(4) The wear path of the Ni coating, as revealed by the wear tests, was found to be wider and deeper compared to that of Ni-TiN thin coatings. But, the Ni-TiN coating prepared with ultrasonic intensity value equivalent to 30 W/cm^2 has the lowest loss of weight and shows the highest abrasion resistance with an average friction coefficient is about 0.39.

ACKNOWLEDGEMENT
This work has been supported by the Natural Science Foundation of China (Granted no. 51974089) and the Department of Education Innovation Strong School Project (Granted no. 2018KTSCX141).

References

1. F. Xia, Q. Li, C. Ma, W. Liu, and Z. Ma, *Ceram. Int.,* 46(6) (2020) 7961.
2. F. Xia, Q. Li, C. Ma, D. Zhao, and Z. Ma, *Int. J. Electrochem. Sci.,* 15 (2020) 1813.
3. M. Jiang, C. Ma, F. Xia, and Y. Zhang, *Surf. Coat. Tech.,* 286 (2016) 191.
4. X. Li, Y. Zhu, and G. Xiao, *Ceram. Int.,* 40 (8) (2014) 11767.
5. J.H. Xue, M.H. Wu, and F.F. Xia, *Surf. Tech.,* 38 (4) (2009) 13. (In Chinese)
6. J.N. Li, and S.L. Gong, *Laser. Eng.,* 27 (5) (2014) 303.
7. H.M. Zhou, X.Y. Hu, and J. Li, *J. Cent. South. Univ.,* 25 (6) (2018) 1350.
8. C. Ma, X. Guo, J. Leang, and F. Xia, *Ceram. Int.,* 42 (8) (2016) 10428.
9. C. Ma, D. Zhao, H. Xia, F. Xia, Z. Ma, and T. Williams, *Int. J. Electrochem. Sci.,* 15 (2020) 4015.
10. F.F. Xia, C. Liu, F. Wang, M.H. Wu, J.D. Wang, H.L. Fu, and J.X. Wang, *J. Alloys. Compd.,* 490 (1-2) (2010) 431.
11. G. Gyawali, B. Joshi, K. Tripathi, and S.W. Lee, *J. Mater. Eng. Perform.,* 26 (9) (2017) 4462.
12. Y. Xu, Y. Zhu, G. Xiao, and C. Ma, *Ceram. Int.,* 40 (4) (2014) 5425.
13. T.S. Han, A.B. Yu, and X.L. Tian, *Chin. Surf. Eng.,* 6 (2012) 32. (In Chinese)
14. Z. Wu, B. Shen, and L. Liu, *Surf. Coat. Tech.,* 206 (14) (2012) 3173.
15. Z. Zhang and Q. Du, *J. Funct. Mater.,* 50(3) (2019) 3081. (In Chinese)
16. F. Xia, W. Jia, M. Jiang, and J. Wang, *Ceram. Int.,* 43 (17) (2017) 14623.

17. F.F. Xia, M.H. Wu, F. Wang, Z.Y. Jia, and A.L. Wang, *Curr. Appl. Phys.,* 9 (1) (2009) 44.
18. S.R. Allahkaram, S. Golroh, and M. Mohammadalipour, *Mater. Des.,* 32 (2011) 4478.
19. L. Wang, Y. Gao, Q. Xue, H. Liu, and T. Xu, *Appl. Surf. Sci.,* 242 (2004) 326.
20. E.P. Georgiou, T.V.D Donck, and J.P. Celis, *T. I. Met. Finish.,* 95 (6) (2017) 301.